Nano Research 2016, 9(12): 3772–3780
DOI 10.1007/s12274-016-1247-y
Research Article
ISSN 1998-0124
CN 11-5974/O4

Interlayer coupling in anisotropic/isotropic van der Waals heterostructures of ReS_2 and MoS_2 monolayers

Mei Zhao[1,§], Wenting Zhang[1,2,§], Manman Liu[1], Chao Zou[1], Keqin Yang[1], Yun Yang[1], Youqing Dong[1], Lijie Zhang[1] (✉), and Shaoming Huang[1] (✉)

[1] *College of Chemistry and Materials Engineering, Wenzhou University, Zhejiang Key Laboratory of Carbon Materials, Wenzhou 325035, China*
[2] *Key Laboratory of Strongly-Coupled Quantum Matter Physics, Chinese Academy of Sciences, School of Physical Sciences, University of Science and Technology of China, Hefei 230026, China*
[§] *These authors contributed equally to this work.*

Received: 21 May 2016
Revised: 28 July 2016
Accepted: 5 August 2016

KEYWORDS
ReS_2/MoS_2 monolayers, van der Waals heterostructures, interlayer coupling interactions, optoelectronics

ABSTRACT

In-plane symmetry is an important contributor to the physical properties of two-dimensional layered materials, as well as atomically thin heterojunctions. Here, we demonstrate anisotropic/isotropic van der Waals (vdW) heterostructures of ReS_2 and MoS_2 monolayers, where interlayer coupling interactions and charge separation were observed by *in situ* Raman–photoluminescence spectroscopy, electrical, and photoelectrical measurements. We believe that these results could be helpful for understanding the fundamental physics of atomically thin vdW heterostructures and creating novel electronic and optoelectronic devices.

1 Introduction

Semiconductor homojunctions and heterojunctions are the crucial building blocks of modern semiconductor devices [1, 2], such as transistors, photodetectors, light emitter diodes, solar cells, and laser diodes [3–5]. The scaling down of conventional semiconductor devices is approaching the limit of miniaturization due to issues such as severe short-channel effects, tunneling effects, and thermal runaway [6]. One solution to this problem is to develop atomically thin semiconductor heterojunctions. Graphene and two-dimensional (2D) transition-metal dichalcogenides (TMDs), with exceptional electronic, optical and mechanical properties, have sparked a revolution in semiconductor materials over the past several years

Address correspondence to Lijie Zhang, zlj4165@126.com; Shaoming Huang, smhuang@wzu.edu.cn

[7–10]. The advances in preparation of these ultrathin materials have pushed the research of atomically thin heterojunctions [11–13]. In the last two years, graphene/h-BN [14, 15], graphene/MX_2 [16, 17], MX_2/MX_2 (MX_2, M = Mo, W; X = S, Se, Te) [18] van der Waals (vdW) monolayer heterostructures (MHSs) have been successfully prepared and offered great potential for fabricating electronic and optoelectronic devices. Most 2D TMDs (MoS_2, $MoSe_2$, $MoTe_2$, WS_2 and WSe_2) that have been studied, e.g., graphene, have demonstrated isotropic behavior due to high lattice symmetry [19]. These MX_2 crystals have the common 2H-lattice structure, in which molybdenum (or tungsten) atoms are sandwiched between two layers of sulfur (or selenium, tellurium) atoms to form a trigonal prismatic lattice. So far, six kinds of MX_2/MX_2 (MoS_2/WS_2, MoS_2/WSe_2, MoS_2/$MoSe_2$, $MoSe_2$/WSe_2, WS_2/WSe_2, MoS_2/$MoTe_2$) [20–25] MHSs have been fabricated via mechanical transfer techniques or a direct chemical vapor deposition (CVD) growth process. Both layers in these MHSs have the same lattice symmetry, implying that their electron transport and linear optical properties are largely analogous in the two atomic layers [19, 26].

Significantly, lowering the in-plane symmetry in 2D ultrathin TMDs could induce interesting anisotropic properties of both electrical and optical responses [27, 28]. To reveal the subtle influence of the asymmetry lattice on the physical properties of ultrathin vdW heterojunctions, it is important to develop atomically thin heterostructures consisting of both in-plane anisotropic TMDs and isotropic TMDs. As a new member of the TMD family, rhenium disulfide (ReS_2) exhibits many exotic properties such as strong in-plane anisotropy, weak interlayer coupling, and lack of an indirect to direct gap transition [29–31]. ReS_2 has a distorted 1T crystal structure due to charge decoupling from an extra valence electron in the d orbital of rhenium atoms [32–34]. ReS_2-based field effect transistors (FETs) and digital devices exhibited excellent electronic performance [35–37]. Hence, ReS_2 offers a favorable platform for studying atomically thin heterojunctions of in-plane anisotropy.

In this work, we report a ReS_2/MoS_2 vdW MHS for the first time. We systematically investigate interlayer-coupled interactions of the anisotropic/isotropic vdW MHS by Raman and photoluminescence (PL) spectroscopy. Moreover, ReS_2/MoS_2 MHS devices were fabricated and exhibited well-defined current rectification behavior. The results verify the charge transfer process at the interface of ReS_2/MoS_2 MHSs. Furthermore, a clear photoresponse was observed under illumination, suggesting potential applications in optoelectronics.

2 Experimental section

2.1 Synthesis of MoS_2 monolayers

A home-built dual-zone CVD horizontal quartz tube furnace was used to grow MoS_2 monolayers. Sulfur powder (99.5%, Sigma-Aldrich) was placed in the center of the first zone at a temperature of 230 ℃. A quartz boat loaded with MoO_3 powder (99.99%, Sigma-Aldrich) was placed in the second zone near the sulfur powder. The distance between sulfur powder and MoO_3 powder was about 20 cm. The growth substrates (285 nm-SiO_2/Si) were placed face down and put directly on top of the MoO_3 powder. The second zone was heated to 700 ℃ and maintained at that temperature for 10 min under an argon flow of 100 sccm followed by natural cooling.

2.2 Fabrication of ReS_2/MoS_2 heterostructures

The ReS_2/MoS_2 vdW heterostructures are fabricated using a mechanical transfer technique. First, MoS_2 monolayers pre-grown by CVD were selected to act as the bottom layer. Next, PMMA/PVA double films were spin-coated onto the Si substrate, and the ReS_2 monolayer crystal was mechanically exfoliated on top of the film.

Using adherent tape to support the hyaline film, the ReS_2 monolayer was transferred onto the target MoS_2 monolayer precisely, under an optical microscope. Finally, the organic film was removed after immersion in acetone.

Metallic contacts were fabricated by standard electron beam lithography, followed by thermal deposition of chromium/gold (8 nm/60 nm), and then a lift-off process.

2.3 Characterization

Optical microscopy (Leica DM4000M), scanning electron microscopy (SEM, FEI NanoSEM 200) and atomic

force microscopy (AFM, Nanoscope IIIa, Vecoo) were used to characterize ReS_2, MoS_2 monolayers (ML-ReS_2 and ML-MoS_2, respectively) and vdW heterostructures. Transmission electron microscopy (TEM, JEOL 2100F) was used to directly identify the crystal structure of ReS_2. *In situ* Raman and PL measurements were performed using a Nanofinder 30 (TII Tokyo Instruments, Inc.) in ambient air at room temperature. The excitation source was a solid-state laser with a wavelength of 532 nm and a power of 2 mW. No significant heating of the samples was observed in the spectral measurements. Raman spectra were calibrated using the Raman shift of single-crystal silicon at 520.4 cm^{-1}. Electrical measurements were performed using a Lake Shore (CRX-6.5K) probe station and a Keithley 4200 semiconductor characterization system. Photoresponse was induced by using a 532-nm laser with a power density of 30.6 $\mu W \cdot cm^{-2}$.

3 Results and discussion

ReS_2 monolayers were mechanically exfoliated from bulk crystals onto Si substrates with a 285-nm SiO_2 layer (Fig. 1(a)). Figure 1(b) shows an AFM image of ReS_2 monolayer in Fig. 1(a). The height profile of the AFM image shows that the thickness of a ReS_2 flake is ~0.78 nm; the thickness corresponds to a unit cell [38]. Most of the exfoliated ReS_2 sheets appear in a parallel quadrilateral shape with inner angles of ~120° or 60° which match the angles between the *a* [100] and *b* [010] axes of ReS_2 (118.97° and 61.03°, respectively) as shown in Fig. 1(c). This behavior can be explained as a result of the weak breaking strength along these two axes [28]. The (100) and (010) lattice planes of the ReS_2 nanosheets are labeled in the high-resolution TEM (HRTEM) image (Fig. 1(c)). The HRTEM image also confirmed the high crystallinity of the as-prepared ReS_2. The selected area electron diffraction (SAED) pattern (inset in Fig. 1(c)) demonstrates the 1T structure and two crystal directions of ReS_2 flakes: [010] and [100] [39].

Numerous Raman vibrational modes were observed in the range of 100–550 cm^{-1} due to the low symmetry of ReS_2. Figure 1(d) shows the Raman spectra of monolayer (ML), multilayer (Multi), and bulk ReS_2 prepared by mechanical exfoliation. It is worth noting

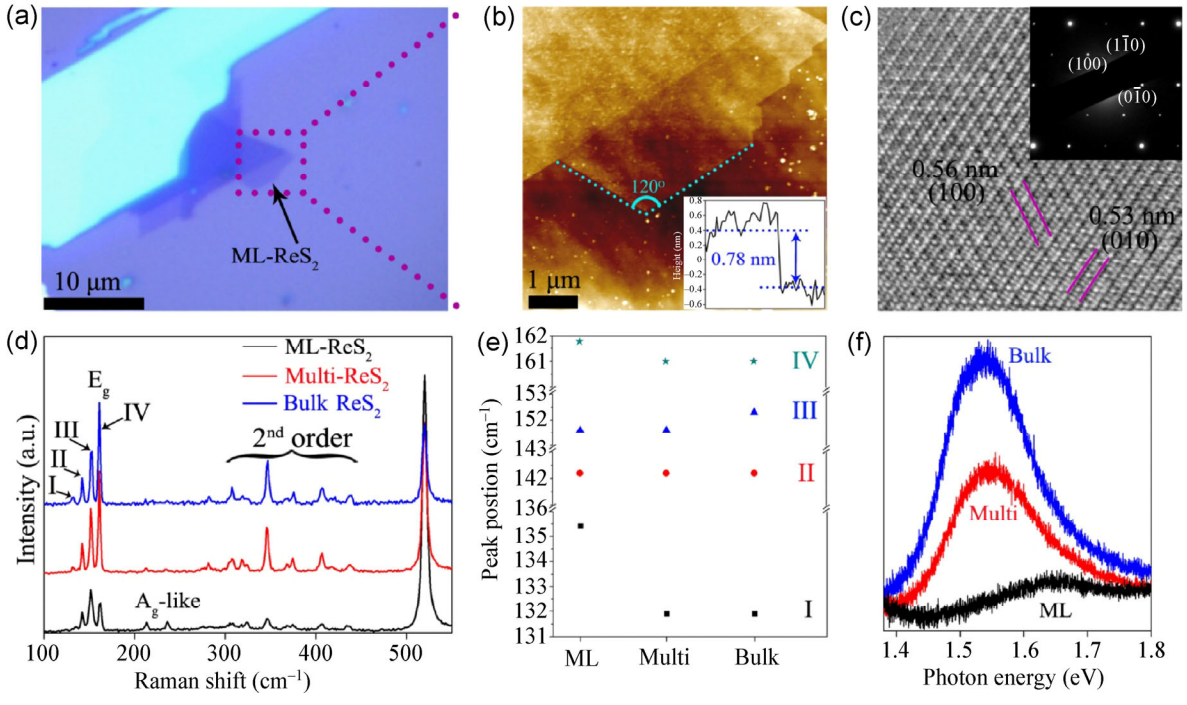

Figure 1 (a) Optical micrograph of an exfoliated ReS_2 monolayer on 285 nm SiO_2/Si substrate (the region within dotted line). (b) *In situ* AFM measurements of the region within dotted line in panel (a). (c) HRTEM image of the ReS_2 flakes. Inset: the SAED pattern of ReS_2 flake. (d) Raman spectra of the exfoliated ML-ReS_2, Multi-ReS_2, and bulk ReS_2. (e) Plot of four Raman peaks in panel (d) for ML-ReS_2, Multi-ReS_2, and bulk ReS_2. (f) PL spectra of the exfoliated ML-ReS_2, Multi-ReS_2, and bulk ReS_2.

that the intensity of most Raman peaks is sensitive to the thickness of flake, whereas the peak positions stay unchanged. This is quite different from other TMDs such as MoS_2, WS_2. We labeled four main vibrational modes of ReS_2 in the range of 100–200 cm^{-1} with Roman numerals I–IV. Figure 1(e) shows the positional changes of the four Raman modes (I–IV) with a change in the thickness. We can see that only Raman mode I shows a significant change with thickness. The peak position value changes from 131.9 cm^{-1} for bulk and stiffens (blue shifts) to 135.4 cm^{-1} of monolayer, whereas the peak positions of II–IV for monolayers are slightly different from the bulk materials (<1.5 cm^{-1}). The results indicated weak interlayer coupling interactions in ReS_2. Figure 1(f) displays PL measurements on bulk, multilayer, and monolayer ReS_2 flakes at room temperature. The bulk and multilayer PL data show a peak at 1.55 eV, and a monolayer PL peak at 1.63 eV. The integrated PL intensity increased with the thickness of the sample. These results indicate that ReS_2 does not have a transition from an indirect bandgap in the bulk to a direct bandgap in monolayers and is consistent with previous studies [40, 41].

Figure 2(a) shows an optical micrograph of a ReS_2/MoS_2 vdW heterostructure prepared by transferring

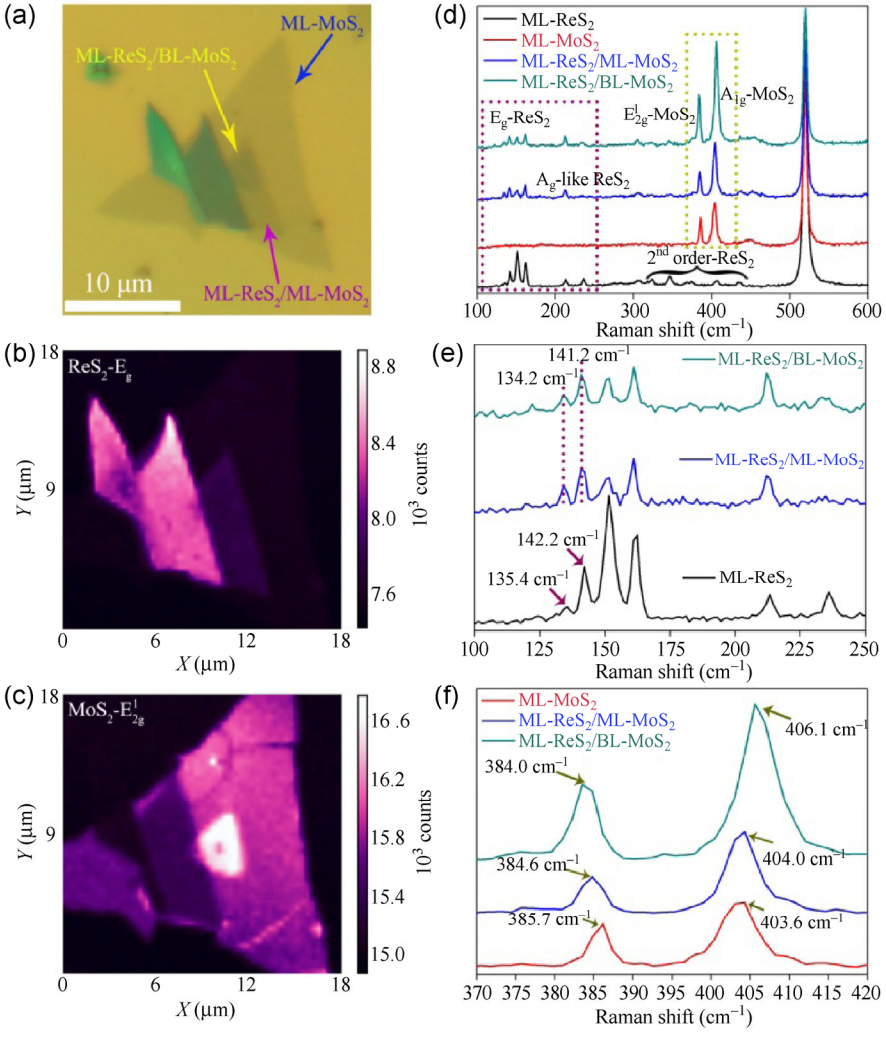

Figure 2 (a) An optical image of ReS_2/MoS_2 vdW heterostructures on 285-nm SiO_2/Si substrate. (b) and (c) Intensity maps of the ReS_2-E_g and MoS_2-E^1_{2g} Raman modes of the sample in panel (a). (d) Raman spectra of the exfoliated ML-ReS_2, the CVD grown ML-MoS_2, and the as-transferred ReS_2/MoS_2 MHS and ML-ReS_2/BL-MoS_2 vdW heterostructures. (e) Raman spectra of zooming panel (d) in the range 100−250 cm^{-1} (i.e., the region within purple dotted line). (f) Raman spectra of zooming panel (d) in the range 370−420 cm^{-1} (i.e., the region within yellow dotted line).

a mechanically exfoliated ReS_2 onto a MoS_2 crystal grown on SiO_2/Si substrate. The region indicated by the purple arrow corresponds to a ML-ReS_2/ML-MoS_2 heterostructure, and the area indicated by the yellow arrow corresponds to a ML-ReS_2/bilayer (BL)-MoS_2 heterostructure. Raman spectroscopy is sensitive to phonon behaviors or the interlayer coupling interaction in layered 2D atomic crystals. Figures 2(b) and 2(c) show Raman intensity mapping of the ReS_2 (E_g mode) and MoS_2 (E^1_{2g} mode), respectively for the sample in Fig. 2(a). Figures 2(d)–2(f) show the corresponding Raman spectra for ReS_2/MoS_2 heterostructures, ML-MoS_2, and ML-ReS_2, respectively. Figure 2(e) clearly displays the change in vibrational modes of ReS_2. Note that two vibrational modes of ReS_2 softened (red shifts) by ~1 cm^{-1} after coupling with MoS_2 monolayers or bilayers. Furthermore, the interlayer coupling interactions also impacted the Raman modes of MoS_2. We found (Fig. 2(f)) that the in-plane (E^1_{2g}) vibrational mode of MoS_2 softened, whereas the out-of-plane (A_{1g}) vibration stiffened after coupling with ReS_2 MLs. The peak frequency difference (Δ) between E^1_{2g} and A_{1g} modes of ML-MoS_2 increased by ~1.5 cm^{-1} after coupling with ML-ReS_2. The variation of Raman modes highlights the interlayer coupling interactions between ReS_2 and MoS_2 heterostructures.

In situ PL spectroscopy and mapping are performed to further verify the interlayer coupling effects in the ReS_2/MoS_2 heterostructures. Figure 3(a) shows the PL spatial mapping of MoS_2 emission at 1.83 eV, corresponding to the sample in Fig. 2(a). We can see that the PL emission from MoS_2 is significantly quenched in the ReS_2/MoS_2 heterostructure area. Figure 3(b) shows the corresponding PL spectra for ML-MoS_2 and ReS_2/MoS_2 heterostructures. The PL intensity of MoS_2 decreased by ~78% in the stacked MHS area compared with bare ML-MoS_2 (line I and II in Fig. 3(b)); the PL peak of ML-ReS_2 could not be observed in areas where the MHSs overlap. The results imply that the charge separation occurred in the heterostructure region. Additionally, the PL quenching shows that type II band alignment probably occurred in the ReS_2/MoS_2 MHS. It is noteworthy that bare ML-MoS_2 had a much stronger PL signal than that of bare BL-MoS_2; however, the ML-MoS_2 showed a much weaker PL peak than BL-MoS_2, after coupling with ML-ReS_2 (line II and III in Fig. 3(b)). The result indicates that the ReS_2/MoS_2 MHS had a more effective charge separation than ML-ReS_2/BL-MoS_2 heterostructures. In addition, the PL peak of MoS_2 blue shifts in the ReS_2/MoS_2 heterostacks. The A exciton and B exciton peaks of MoS_2 PL spectra arose from the direct band gap and strong spin–orbit coupling. We fitted the three PL spectra in Fig. 3(b), as shown in Fig. 3(c). The A exciton and B exciton peaks of ML-MoS_2 blue shifted by 17 and 30 meV, respectively after coupling with ReS_2 monolayers. The blue shifts of the PL peaks for ML-MoS_2 are an interesting phenomenon, and the reason for this is not completely understood until now. A possible mechanism is that the blue shifts are due to strain effects and charge transfer in the interface induced by the top ML-ReS_2. In order to exclude the influence of the covered ML-ReS_2 on the outgoing light (PL emission) from the bottom ML-MoS_2 layer

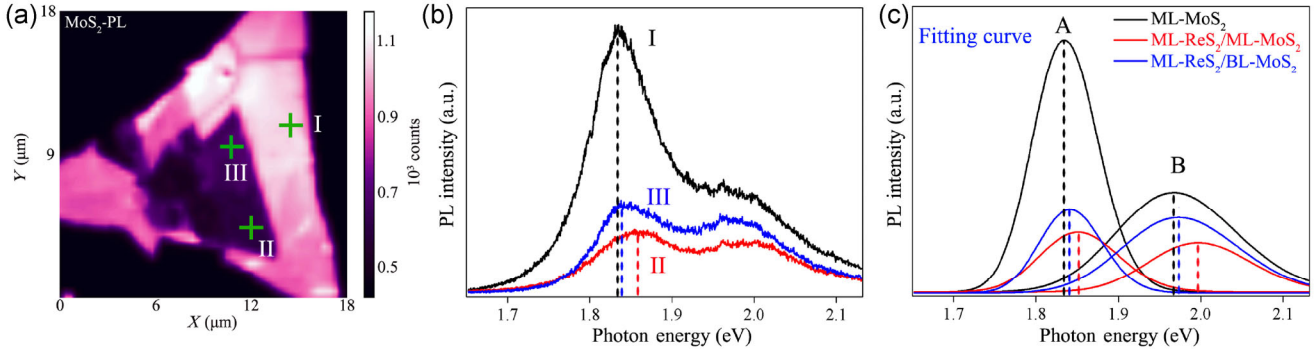

Figure 3 (a) PL intensity map of the emission at about 1.83 eV (MoS_2) for the sample in Fig. 2(a). (b) PL spectra in the range of 1.65−2.13 eV for the three regions indicated in panel (a): ML-MoS_2 (I), ReS_2/MoS_2 vdW MHS (II), and ML-ReS_2/BL-MoS_2 vdW heterostructures (III). (c) The fitted A and B exciton peaks of MoS_2 correspond to the three PL spectra in panel (b).

in the heterostructure area, we also prepared ML-MoS_2/ML-ReS_2 vdW heteostructures (MoS_2/ReS_2 MHS) on SiO_2 (285-nm)/Si substrates, in which ML-MoS_2 was on top of ML-ReS_2, by a mechanical transfer technique. Note that both layers were dissociated from bulk crystals by mechanical exfoliation. Interestingly, the intensity of the PL emission peak of MoS_2 is dramatically quenched in the MoS_2/ReS_2 MHS region as well, as shown in Fig. S2 (in the Electronic Supplementary Material (ESM)). This is consistent with the ReS_2/MoS_2 MHS in which ML-MoS_2 was covered with ML-ReS_2. The results further confirm effective charge separation in the heterostructure, as mentioned above.

To acquire more information about the junction characteristics, we carried out electrical and photoelectric measurements on ReS_2/MoS_2 heterostructure devices. Figure 4(a) shows a schematic illustration of the vdW MHS device of ReS_2/MoS_2. Before testing the electrical characteristics of the ReS_2/MoS_2 heterojunction, we have first characterized the electrical transport properties of ML-MoS_2 and ML-ReS_2 to ensure Ohmic contacts were formed. To this end, the ML-MoS_2 and ML-ReS_2 field effect transistors were fabricated on Si/SiO_2 substrate, with Cr/Au thin film as the source–drain contacts, and the silicon substrate as back-gate electrodes. Figures 4(b) and 4(c) show the I_{ds}–V_{ds} characteristics of ML-MoS_2 and ML-ReS_2 as a function of back gate voltages, respectively. A linear I_{ds}–V_{ds} relationship was observed for both MoS_2 and ReS_2 layers, implying that Ohmic contacts were formed in both materials. Figure 4(d) and Fig. S3(b) (in the ESM) show the transfer characteristics of the ML-ReS_2 and ML-MoS_2 devices exhibiting strong n-type semiconductor behavior. We continued to explore the electrical transport properties of the ReS_2/MoS_2 MHS. A clear current rectification behavior was observed in (I_{ds}–V_{ds}) plots for the MHS device (Fig. 4(e)). The observation of current rectification clearly demonstrated that a diode was formed within the atomically thin ReS_2/MoS_2 heterojunction. In addition, the device based on the ML-MoS_2/ML-ReS_2 heterostructure exhibited excellent gate-modulated transport characteristics, and a high ON/OFF ratio (up to 10^6) was observed in the transfer curve, as shown in Figs. S3(c) and S3(d) in the ESM. Moreover, we evaluated the photocurrent properties of these devices using a 532 nm laser. It is evident that a clear photoresponse is observed under light conditions, as shown in Fig. 4(e). The responsivity (R_λ) is an important parameter for an optoelectronic device. The responsivity of the device was calculated to be 35.07 A·W^{-1} (V_{ds} = 2 V, V_g = 0 V) using the formula: $R_\lambda = I_{ph}/PS$, where $I_{ph} = I_{light} - I_{dark}$, S is the effective area under incident light, and P is the light intensity

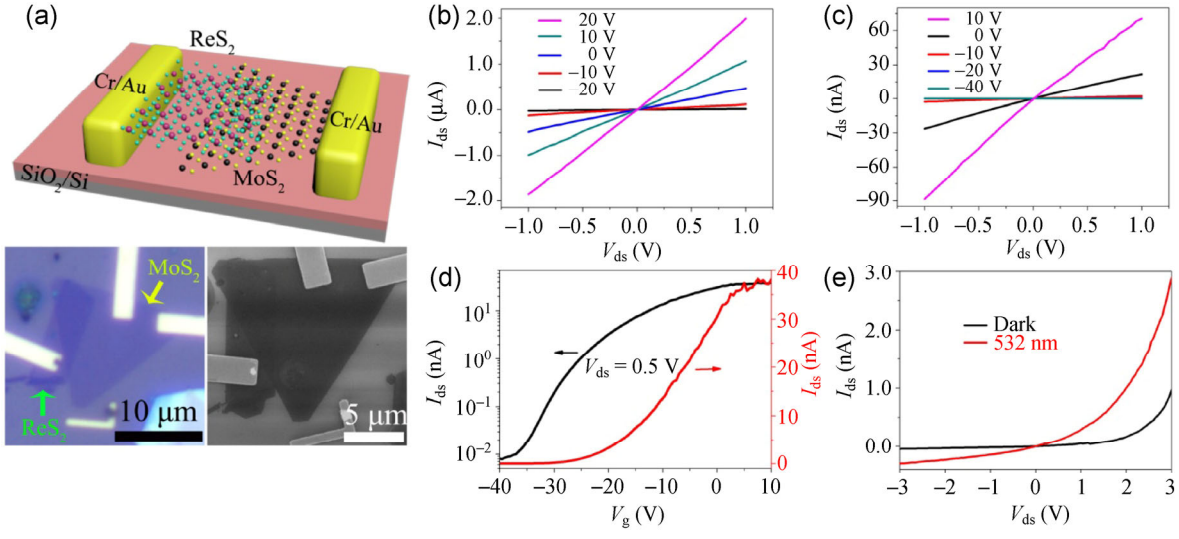

Figure 4 (a) Top: schematic diagram of a ReS_2/MoS_2 vdW heterostructure device. Bottom left and right: optical and SEM micrograph of the fabricated ReS_2/MoS_2 MHS device. (b) The I_{ds}–V_{ds} characteristics of ML-MoS_2 FET transistor. (c) The I_{ds}–V_{ds} characteristics of ML-ReS_2 FET transistor. (d) Transfer characteristics of the ML-ReS_2 FET transistor. (e) Experimental I_{ds}–V_{ds} of ReS_2/MoS_2 vdW MHS device curves in the dark (black line) and under light illumination (532 nm).

(30.6 μW·cm^{-2}). The responsivity determined in this work is higher than that of the heteostructures composed of in-plane isotropic 2D crystals such as few-layer MoS_2/WS_2 vertical heterojunction arrays (2.3 A·W^{-1}) [42], multilayer MoS_2/WS_2 vdW heterostructure (1.42 A·W^{-1}) [43], few-layer α-$MoTe_2/MoS_2$ heterojunction (322 mA·W^{-1} for blue and 37 mA·W^{-1} for 800-nm photons) [44], and other vdW heterostructures such as $GaSe/MoSe_2$ (30 mA·W^{-1}) [45] and $GaTe/MoS_2$ (1.365 A·W^{-1}) [46]. These photoelectrical measurements clearly demonstrate that the ReS_2/MoS_2 vdW heterostructures exhibit excellent photoresponse properties and are promising candidates for fabricating optoelectronic devices.

4 Conclusions

In summary, for the first time, ReS_2/MoS_2 vdW heterojunctions are fabricated with atomically thin geometry and are also atomically sharp. The interlayer coupling interactions of the anisotropic/isotropic vdW heterostructures have been demonstrated by Raman and PL spectroscopy. The electrical and photoelectrical measurements also demonstrate excellent electrical and photoresponse properties in typical ReS_2/MoS_2 heterostacks. We believe that our studies offer an interesting platform for fundamental investigations of the interlayer coupling of anisotropic/isotropic vdW heterostructures, and will be valuable for fabricating flexible and transparent optoelectronic devices in the future.

Acknowledgements

This work was supported by the National Natural Science Foundation of China (Nos. 61471270, 51420105002, and 51572199).

Electronic Supplementary Material: Supplementary material (DFT-calculated results, PL measurements of mechanically exfoliated ML-MoS_2 and MoS_2/ReS_2 MHS, electrical transport properties of MoS_2 and ML-MoS_2/ML-ReS_2 heterostructures) is available in the online version of this article at http://dx.doi.org/10.1007/s12274-016-1247-y.

References

[1] Ohno, Y.; Young, D. K.; Beschoten, B.; Matsukura, F.; Ohno, H.; Awschalom, D. D. Electrical spin injection in a ferromagnetic semiconductor heterostructure. *Nature* **1999**, *402*, 790–792.

[2] Sze, S. M.; Ng, K. K. *Physics of Semiconductor Devices*, 3rd ed.; John Wiley & Sons Inc.: Hoboken, New Jersey, 2007.

[3] Morkoç, H.; Mohammad, S. N. High-luminosity blue and blue-green gallium nitride light-emitting diodes. *Science* **1995**, *267*, 51–55.

[4] Kroemer, H. Heterostructure bipolar transistors and integrated circuits. *Proc. IEEE* **1982**, *70*, 13–25.

[5] Bhattacharya, P. *Semiconductor Optoelectronic Devices*; Prentice Hall: Englewood Cliffs, N.J., 1994.

[6] Ferain, I.; Colinge, C. A.; Colinge, J. P. Multigate transistors as the future of classical metal-oxide-semiconductor field-effect transistors. *Nature* **2011**, *479*, 310–316.

[7] Geim, A. K. Graphene: Status and prospects. *Science* **2009**, *324*, 1530–1534.

[8] Najmaei, S.; Liu, Z.; Zhou, W.; Zou, X. L.; Shi, G.; Lei, S. D.; Yakobson, B. I.; Idrobo, J. C.; Ajayan, P. M.; Lou, J. Vapour phase growth and grain boundary structure of molybdenum disulphide atomic layers. *Nat. Mater.* **2013**, *12*, 754–759.

[9] Chhowalla, M.; Shin, H. S.; Eda, G.; Li, L. J.; Loh, K. P.; Zhang, H. The chemistry of two-dimensional layered transition metal dichalcogenide nanosheets. *Nat. Chem.* **2013**, *5*, 263–275.

[10] Sangwan, V. K.; Jariwala, D.; Kim, I. S.; Chen, K. S.; Marks, T. J.; Lauhon, L. J.; Hersam, M. C. Gate-tunable memristive phenomena mediated by grain boundaries in single-layer MoS_2. *Nat. Nanotechnol.* **2015**, *10*, 403–406.

[11] Geim, A. K.; Grigorieva, I. V. Van der Waals heterostructures. *Nature* **2013**, *499*, 419–425.

[12] Li, H. M.; Lee, D.; Qu, D. S.; Liu, X. C.; Ryu, J. J.; Seabaugh, A.; Yoo, W. J. Ultimate thin vertical p–n junction composed of two-dimensional layered molybdenum disulfide. *Nat. Commun.* **2015**, *6*, 6564.

[13] Liu, L.; Park, J.; Siegel, D. A.; McCarty, K. F.; Clark, K. W.; Deng, W.; Basile, L.; Idrobo, J. C.; Li, A. P.; Gu, G. Heteroepitaxial growth of two-dimensional hexagonal boron nitride templated by graphene edges. *Science* **2014**, *343*, 163–167.

[14] Dean, C. R.; Wang, L.; Maher, P.; Forsythe, C.; Ghahari, F.; Gao, Y.; Katoch, J.; Ishigami, M.; Moon, P.; Koshino, M. et al. Hofstadter's butterfly and the fractal quantum Hall effect in moiré superlattices. *Nature* **2013**, *497*, 598–602.

[15] Sutter, P.; Huang, Y.; Sutter, E. Nanoscale integration of two-dimensional materials by lateral heteroepitaxy. *Nano Lett.* **2014**, *14*, 4846–4851.

[16] Britnell, L.; Ribeiro, R. M.; Eckmann, A.; Jalil, R.; Belle, B. D.; Mishchenko, A.; Kim, Y. J.; Gorbachev, R. V.; Georgiou, T.; Morozov, S. V. et al. Strong light-matter interactions in heterostructures of atomically thin films. *Science* **2013**, *340*, 1311–1314.

[17] Yu, W. J.; Li, Z.; Zhou, H. L.; Chen, Y.; Wang, Y.; Huang, Y.; Duan, X. F. Vertically stacked multi-heterostructures of layered materials for logic transistors and complementary inverters. *Nat. Mater.* **2013**, *12*, 246–252.

[18] Lee, C. H.; Lee, G. H.; van der Zande, A. M.; Chen, W. C.; Li, Y. L.; Han, M. Y.; Cui, X.; Arefe, G.; Nuckolls, C.; Heinz, T. F. et al. Atomically thin p–n junctions with van der Waals heterointerfaces. *Nat. Nanotechnol.* **2014**, *9*, 676–681.

[19] Wang, Q. H.; Kalantar-Zadeh, K.; Kis, A.; Coleman, J. N.; Strano, M. S. Electronics and optoelectronics of two-dimensional transition metal dichalcogenides. *Nat. Nanotechnol.* **2012**, *7*, 699–712.

[20] Gong, Y. J.; Lin, J. H.; Wang, X. L.; Shi, G.; Lei, S. D.; Lin, Z.; Zou, X. L.; Ye, G. L.; Vajtai, R.; Yakobson, B. I. et al. Vertical and in-plane heterostructures from WS_2/MoS_2 monolayers. *Nat. Mater.* **2014**, *13*, 1135–1142.

[21] Duan, X. D.; Wang, C.; Shaw, J. C.; Cheng, R.; Chen, Y.; Li, H. L.; Wu, X. P.; Tang, Y.; Zhang, Q. L.; Pan, A. L. et al. Lateral epitaxial growth of two-dimensional layered semiconductor heterojunctions. *Nat. Nanotechnol.* **2014**, *9*, 1024–1030.

[22] Huang, C. M.; Wu, S. F.; Sanchez, A. M.; Peters, J. J. P.; Beanland, R.; Ross, J. S.; Rivera, P.; Yao, W.; Cobden, D. H.; Xu, X. D. Lateral heterojunctions within monolayer $MoSe_2$–WSe_2 semiconductors. *Nat. Mater.* **2014**, *13*, 1096–1101.

[23] Lui, C. H.; Ye, Z. P.; Ji, C.; Chiu, K. C.; Chou, C. T.; Andersen, T. I.; Means-Shively, C.; Anderson, H.; Wu, J. M.; Kidd, T. et al. Observation of interlayer phonon modes in van der Waals heterostructures. *Phys. Rev. B* **2015**, *91*, 165403.

[24] Furchi, M. M.; Pospischil, A.; Libisch, F.; Burgdorfer, J.; Mueller, T. Photovoltaic effect in an electrically tunable van der Waals heterojunction. *Nano Lett.* **2014**, *14*, 4785–4791.

[25] Zhang, K. A.; Zhang, T. N.; Cheng, G. H.; Li, T. X.; Wang, S. X.; Wei, W.; Zhou, X. H.; Yu, W. W.; Sun, Y.; Wang, P. et al. Interlayer transition and infrared photodetection in atomically thin type-II $MoTe_2$/MoS_2 van der Waals heterostructures. *ACS Nano* **2016**, *10*, 3852–3858.

[26] Huang, X.; Zeng, Z. Y.; Zhang, H. Metal dichalcogenide nanosheets: Preparation, properties and applications. *Chem. Soc. Rev.* **2013**, *42*, 1934–1946.

[27] Ali, M. N.; Xiong, J.; Flynn, S.; Tao, J.; Gibson, Q. D.; Schoop, L. M.; Liang, T.; Haldolaarachchige, N.; Hirschberger, M.; Ong, N. P. et al. Large, non-saturating magnetoresistance in WTe_2. *Nature* **2014**, *514*, 205–208.

[28] Liu, E. F.; Fu, Y. J.; Wang, Y. J.; Feng, Y. Q.; Liu, H. M.; Wan, X. G.; Zhou, W.; Wang, B. G.; Shao, L. B.; Ho, C. H. et al. Integrated digital inverters based on two-dimensional anisotropic ReS_2 field-effect transistors. *Nat. Commun.* **2015**, *6*, 6991.

[29] Tongay, S.; Sahin, H.; Ko, C.; Luce, A.; Fan, W.; Liu, K.; Zhou, J.; Huang, Y. S.; Ho, C. H.; Yan, J. Y. et al. Monolayer behaviour in bulk ReS_2 due to electronic and vibrational decoupling. *Nat. Commun.* **2014**, *5*, 3252.

[30] Cui, Q. N.; Zhao, H. Coherent control of nanoscale ballistic currents in transition metal dichalcogenide ReS_2. *ACS Nano* **2015**, *9*, 3935–3941.

[31] Keyshar, K.; Gong, Y. J.; Ye, G. L.; Brunetto, G.; Zhou, W.; Cole, D. P.; Hackenberg, K.; He, Y. M.; Machado, L.; Kabbani, M. et al. Chemical vapor deposition of monolayer rhenium disulfide (ReS_2). *Adv. Mater.* **2015**, *27*, 4640–4648.

[32] Feng, Y. Q.; Zhou, W.; Wang, Y. J.; Zhou, J.; Liu, E. F.; Fu, Y. J.; Ni, Z. H.; Wu, X. L.; Yuan, H. T.; Miao, F. et al. Raman vibrational spectra of bulk to monolayer ReS_2 with lower symmetry. *Phys. Rev. B* **2015**, *92*, 054110.

[33] He, R.; Yan, J. A.; Yin, Z. Y.; Ye, Z. P.; Ye, G. H.; Cheng, J.; Li, J.; Lui, C. H. Coupling and stacking order of ReS_2 atomic layers revealed by ultralow-frequency Raman spectroscopy. *Nano Lett.* **2016**, *16*, 1404–1409.

[34] Pradhan, N. R.; McCreary, A.; Rhodes, D.; Lu, Z. G.; Feng, S. M.; Manousakis, E.; Smirnov, D.; Namburu, R.; Dubey, M.; Walker, A. R. H. et al. Metal to insulator quantum-phase transition in few-layered ReS_2. *Nano Lett.* **2015**, *15*, 8377–8384.

[35] Yang, S. X.; Kang, J.; Yue, Q.; Coey, J. M. D.; Jiang, C. B. Defect-modulated transistors and gas-enhanced photodetectors on ReS_2 nanosheets. *Adv. Mater. Interfaces* **2016**, *3*, 1500707.

[36] Corbett, C. M.; McClellan, C.; Rai, A.; Sonde, S. S.; Tutuc, E.; Banerjee, S. K. Field effect transistors with current saturation and voltage gain in ultrathin ReS_2. *ACS Nano* **2015**, *9*, 363–370.

[37] Liu, E. F.; Long, M. S.; Zeng, J. W.; Luo, W.; Wang, Y. J.; Pan, Y. M.; Zhou, W.; Wang, B. G.; Hu, W. D.; Ni, Z. H. et al. High responsivity phototransistors based on few-layer ReS_2 for weak signal detection. *Adv. Funct. Mater.* **2016**, *26*, 1938–1944.

[38] Liu, F. C.; Zheng, S. J.; He, X. X.; Chaturvedi, A.; He, J. F.; Chow, W. L.; Mion, T. R.; Wang, X. L.; Zhou, J. D.; Fu, Q. D. et al. Highly sensitive detection of polarized light using anisotropic 2D ReS_2. *Adv. Funct. Mater.* **2016**, *26*, 1169–1177.

[39] Lin, Y. C.; Komsa, H. P.; Yeh, C. H.; Björkman, T.; Liang, Z. Y.; Ho, C. H.; Huang, Y. S.; Chiu, P. W.; Krasheninnikov, A. V.; Suenaga, K. Single-layer ReS_2: Two-dimensional semiconductor with tunable in-plane anisotropy. *ACS Nano* **2015**, *9*, 11249–11257.

[40] Cui, Q. N.; He, J. Q.; Bellus, M. Z.; Mirzokarimov, M.; Hofmann, T.; Chiu, H. Y.; Antonik, M.; He, D. W.; Wang, Y. S.; Zhao, H. Transient absorption measurements on anisotropic monolayer ReS_2. *Small* **2015**, *11*, 5565–5571.

[41] He, X. X.; Liu, F. C.; Hu, P.; Fu, W.; Wang, X. L.; Zeng, Q. S.; Zhao, W.; Liu, Z. Chemical vapor deposition of high-quality and atomically layered ReS_2. *Small* 2015, *11*, 5423–5429.

[42] Xue, Y. Z.; Zhang, Y. P.; Liu, Y.; Liu, H. T.; Song, J. C.; Sophia, J.; Liu, J. Y.; Xu, Z. Q.; Xu, Q. Y.; Wang, Z. Y. et al. Scalable production of a few-layer MoS_2/WS_2 vertical heterojunction array and its application for photodetectors. *ACS Nano* 2016, *10*, 573–580.

[43] Huo, N. J.; Kang, J.; Wei, Z. M.; Li, S. S.; Li, J. B.; Wei, S. H. Novel and enhanced optoelectronic performances of multilayer MoS_2–WS_2 heterostructure transistors. *Adv. Funct. Mater.* 2014, *24*, 7025–7031.

[44] Pezeshki, A.; Hossein, S.; Shokouh, H.; Nazari, T.; Oh, K.; Im, S. Electric and photovoltaic behavior of a few-layer α-$MoTe_2/MoS_2$ dichalcogenide heterojunction. *Adv. Mater.* 2016, *28*, 3216–3222.

[45] Li, X.; Lin, M. W., Lin, J.; Huang, B.; Puretzky, A. A.; Ma, C.; Wang, K.; Zhou, W.; Pantelides, S. T.; Chi, M. et al. Two-dimensional GaSe/$MoSe_2$ misfit bilayer heterojunctions by van der Waals epitaxy. *Sci. Adv.* 2016, *2*, e1501882.

[46] Yang, S. X.; Wang, C.; Ataca, C., Li, Y.; Chen, H.; Cai, H.; Suslu, A.; Grossman, J. C.; Jiang, C. B.; Liu, Q. et al. Self-driven photodetector and ambipolar transistor in atomically thin GaTe-MoS_2 p–n vdW heterostructure. *ACS Appl. Mater. Interfaces* 2016, *8*, 2533–2539.